Article

Structural Influence and Interactive Binding Behavior of Dopamine and Norepinephrine on the Greek-Key-Like Core of α-Synuclein Protofibril Revealed by Molecular Dynamics Simulations

Yu Zou [1,†], Zhiwei Liu [2,†], Zhiqiang Zhu [2] and Zhenyu Qian [2,*]

[1] Department of Sport and Exercise Science, College of Education, Zhejiang University, 148 Tianmushan Road, Hangzhou 310007, China; zouyu_1993@163.com

[2] Key Laboratory of Exercise and Health Sciences (Ministry of Education) and School of Kinesiology, Shanghai University of Sport, 399 Changhai Road, Shanghai 200438, China; liuzhiwei_1995@163.com (Z.L.); zzq5819@163.com (Z.Z.)

[*] Correspondence: qianzhenyu@sus.edu.cn

[†] Y.Z. and Z.L. contributed equally to this work.

check for updates

Abstract: The pathogenesis of Parkinson's disease (PD) is closely associated with the aggregation of α-synuclein (αS) protein. Finding the effective inhibitors of αS aggregation has been considered as the primary therapeutic strategy for PD. Recent studies reported that two neurotransmitters, dopamine (DA) and norepinephrine (NE), can effectively inhibit αS aggregation and disrupt the preformed αS fibrils. However, the atomistic details of αS-DA/NE interaction remain unclear. Here, using molecular dynamics simulations, we investigated the binding behavior of DA/NE molecules and their structural influence on αS_{44-96} (Greek-key-like core of full length αS) protofibrillar tetramer. Our results showed that DA/NE molecules destabilize αS protofibrillar tetramer by disrupting the β-sheet structure and destroying the intra- and inter-peptide E46–K80 salt bridges, and they can also destroy the inter-chain backbone hydrogen bonds. Three binding sites were identified for both DA and NE molecules interacting with αS tetramer: T54–T72, Q79–A85, and F94–K96, and NE molecules had a stronger binding capacity to these sites than DA. The binding of DA/NE molecules to αS tetramer is dominantly driven by electrostatic and hydrogen bonding interactions. Through aromatic π-stacking, DA and NE molecules can bind to αS protofibril interactively. Our work reveals the detailed disruptive mechanism of protofibrillar αS oligomer by DA/NE molecules, which is helpful for the development of drug candidates against PD. Given that exercise as a stressor can stimulate DA/NE secretion and elevated levels of DA/NE could delay the progress of PD, this work also enhances our understanding of the biological mechanism by which exercise prevents and alleviates PD.

Keywords: amyloid protofibril; small molecules; protein–ligand interaction; inhibitory mechanism; molecular dynamics simulation

1. Introduction

Peptide self-assembly into amyloid fibrillar aggregates is associated with several neurodegenerative disorders, including Parkinson's disease (PD), Alzheimer's disease, and Huntington's disease [1–3]. The main component of the amyloid-rich Lewy bodies found abundantly throughout the PD brain is α-synuclein (αS) protein, whose fibrillation is crucially involved in PD [4,5]. The mature αS fibril has a common amyloid feature of a cross-β spine with β-strands perpendicular to the fibril axis [6,7]. The formation of αS fibrils is characterized by a nucleation-elongation process, in which the fibrils

grow rapidly through the addition of monomers once a nucleus is formed [8,9]. Although αS fibrils are thought to be the toxic species responsible for PD, recent studies have shown that soluble small oligomers are more cytotoxic than mature fibrils [10,11]. Thus, reducing the oligomeric species is an effective way to prevent αS aggregation.

A number of strategies of molecular intervention to reduce the toxic effects of these oligomeric aggregates of αS have been proposed. Several potential inhibitors, including short peptides [12,13], small molecules [14,15], antibodies [16,17], and nanoparticles [18,19], are reported to be able to impede αS aggregation and dissociate preformed fibrils. Among these inhibitors, two neurotransmitters, dopamine (DA) and norepinephrine (NE), have gained great attention due to their remarkable ability to inhibit amyloid aggregation. In the brain, DA exerts its effect through DA receptors (D1–D5), and its deficiency is the main feature of PD [20,21]. The release of NE exerts a potent neuromodulatory effect on synaptic transmission, and the additional loss of NE neurons in the locus coeruleus is related to the motor and non-motor deficits in PD [22,23]. In the last two decades, experimental researchers have focused on the mechanisms by which DA/NE molecules inhibit αS aggregation or disrupt the preformed αS protofibrils [24–37]. Conway et al. screened 169 drug-like compounds, and first found that catecholamines (including DA/NE) have the ability to inhibit αS fibrillization [24]. Using the combined methods of the thioflavin T assay, light scattering, electron microscopy, and atomic force microscopy, Li et al. showed that micromolar concentrations of DA/NE can both prevent the formation of αS fibrils and dissolve pre-existing fibrils [25]. Matera et al. reported that in the presence of DA/NE molecules, the fibrillar content of αS is able to decrease to 20–40% of the initial amount compared to the αS solution alone [32]. Illes-Toth et al. suggested that DA can induce the population of a highly extended state of αS and modulate αS self-assembly [35]. In the cytotoxicity tests, Singh et al. proposed that NE has a weak binding to the initial and intermediate states of the αS fibrillation pathway, which may promote the production of cytotoxic species [37]. Morshedi et al. found that simultaneous treatment of cultured PC12 cells with DA and early stage αS aggregates can significantly increase the viability of cells in comparison with each treatment alone [38]. Despite these experimental studies, the influence of DA/NE molecules on αS aggregation at the atomistic level is still elusive.

In this study, we carried out all-atom molecular dynamics (MD) simulations to investigate the detailed interactions and underlying disruptive mechanisms of DA/NE molecules with αS_{44-96} protofibrillar oligomer. Previous study showed that the αS_{44-96} fragment is the ordered core region of the full length αS fibril, and its structure adopts a β-serpentine arrangement with a β-sheet-rich Greek-key-like topology [39]. It was reported that catecholamines could bind preferentially to 125YEMPS129 residues in the C-terminal region and non-amyloid component region [27,28,33,40–42]. As we are concerned mostly with the general properties of in-registry parallel β-sheet amyloids rather than αS itself, the αS_{44-96} region (consisting of 53 residues) is chosen as our simulated model. DA/NE molecules are simultaneously added around the αS protein in the same simulation system. We did so because DA/NE molecules co-exist in the brain. They are synthesized from the same precursor (amino acid tyrosine) and have high structural similarity. The concomitant loss of DA and NE could promote aberrant motor and non-motor symptoms of PD, which suggests that the two compounds are closely related in the brain [43–45]. Besides, experimental studies showed that DA/NE molecules can both effectively inhibit the αS fibrillization and decrease the toxicity of αS aggregates [24,25,32,38]. It is interesting to examine the similarity and difference of the interactions of DA/NE molecules with αS, as well as the interactivity of DA/NE. Our MD simulations show that DA/NE molecules can destabilize αS protofibrillar tetramer by disrupting the β-sheet structure and destroying the intra- and inter-peptide E46-K80 salt bridges. Both DA and NE molecules have a high binding affinity at three sites of αS tetramer. The electrostatic and hydrogen bonding interactions play dominant roles in DA/NE molecules disrupting αS protofibrils. The aromatic π-stacking helps DA and NE molecules bind to αS protofibril interactively.

2. Materials and Methods

2.1. αS_{44-96} Tetramer and DA/NE Molecules

The amino acid sequence of αS_{44-96} peptide is [44]TKEGVVH[50]GVATVAEKTK[60]E QVTNVGGAV[70]VTGVTAVAQK[80]TVEGAGSIAA[90]ATGFVK[96]. The initial coordinate of the αS tetramer was taken from the αS fibril structure (PDB ID: 2N0A) resolved by solid-state nuclear magnetic resonance (NMR) [39]. Residues 1–43 and 97–140 were removed from the original structure to construct the Greek-key-like core region of αS (αS_{44-96}). The structures of the DA/NE molecules were taken from the ChemSpider database, and the topologies of the DA/NE molecules were obtained by the GlycoBioChem PRODRG2 Server [46]. The geometry structures of DA/NE molecules were first optimized using Spartan'10 [47] and then energy-minimized by GAMESS software [48]. The partial charges of DA/NE atoms were generated by the Amber Tools REP package [49]. In aqueous solutions at a pH $\approx$ 7.0, DA/NE molecules mostly adopt the protonated amino groups [50]. Therefore, positively charged protonated DA and NE molecules were considered in our simulations. The cytotoxicity of NE bound (in its oxidized form) αS oligomers remains controversial, which deserves further investigation [32,37]. The molar ratio of DA/NE molecules to αS peptide chains is 2:1, which is equal to that used in the experimental study [32]. DA/NE molecules co-exist in the brain, and the concentration of NE is much higher than that of DA [51,52]. For easy comparison, we took the αS tetramer system containing an equal quantity of DA and NE molecules as a model system in our simulations. Two systems were simulated: an isolated αS_{44-96} protofibrillar tetramer (named the tetramer system) and an αS_{44-96} protofibrillar tetramer in the presence of four DA and four NE molecules (named the tetramer + DA/NE system). In the initial state of the tetramer + DA/NE system, DA/NE molecules were simultaneously placed around αS_{44-96} (αS for short) protofibrillar tetramer, with a minimum distance of >1.5 nm [32]. The initial states of simulated systems and the molecular structures of DA/NE are displayed in Figure 1. The initial conditions of three MD runs for isolated αS tetramer were exactly the same except for the initial velocities of atoms. The velocities were generated according to Maxwell's distribution at 310 K.
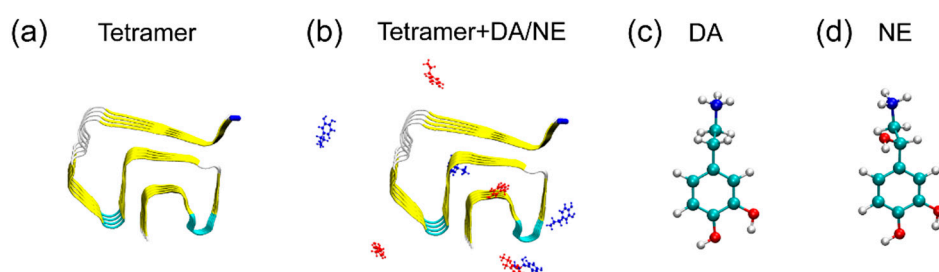
Figure 1. (**a**,**b**) Initial states of αS tetramer and tetramer in the absence and presence of DA/NE (dopamine/norepinephrine) molecules. DA and NE molecules are colored in red and blue, respectively. The Cα-atom of the N-terminal residue T44 in each αS peptide is represented by a blue bead. (**c**,**d**) Chemical structures of DA and NE molecules. Color codes: carbon atoms (cyan), oxygen atoms (red), nitrogen atoms (blue), and hydrogen atoms (white).

2.2. MD Simulation Details

All MD simulations were performed in the isothermal-isobaric (NPT) ensemble using the GROMACS-5.1.4 software package [53] with the Amber 99SB-ILDN force field [54]. The systems were solvated in a $7.45 \times 7.45 \times 7.45$ nm^3 cubic box with TIP3P water molecules [55]. Na$^+$ and Cl$^-$ ions were both added to neutralize the systems, providing an additional 0.1 M salt concentration. The net charges of the αS_{44-96} peptide and DA/NE molecules were separately +2 and +1/+1 at neutral pH; thus, more counterions (Cl$^-$) were added to neutralize the two systems. Constraints were applied for bond lengths of peptides using the LINCS algorithm [56] and for the water molecules using SETTLE algorithms [57]. The pressure was kept at 1 bar using the Parrinello–Rahman method [58] with a coupling time constant

of 1.0 ps. The temperature was kept at 310 K using the velocity rescaling coupling method with a coupling constant of 0.1 ps. Long-range electrostatic interaction was described by the particle mesh Ewald (PME) method [59] with a real space cutoff of 1.2 nm. The cutoff for van der Waals interactions was 1.2 nm. Three independent 300 ns MD simulations were conducted for αS tetramer with DA/NE molecules, and three 300 ns MD simulations without DA/NE molecules were performed as a control.
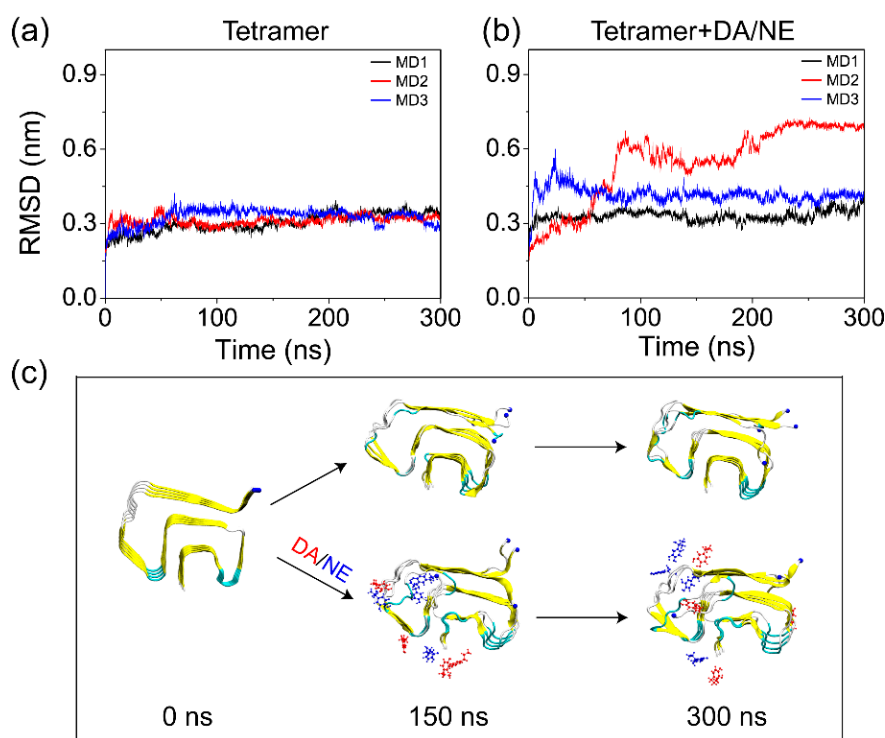
2.3. Analysis

MD trajectories were analyzed by the facilities of the GROMACS-5.1.4 software package and in-house developed codes. The DSSP program [60] was used to calculate the protein secondary structure. One hydrogen bond (H-bond) was taken as formed if the N···O distance was less than 0.35 nm and the N-H···O angle was greater than 150°. Previous studies reported that an ion pair can be defined as a salt bridge if the centroids of the side-chain charged-group atoms in the residues (Asp or Glu with Arg, Lys, or His) lie within 4.0 Å of each other, and at least one pair of Asp or Glu side-chain carbonyl oxygen and side-chain nitrogen atom of Arg, Lys, or His is also within this distance [61–63]. This criterion has been widely used in many computational studies [64–67]. Therefore, in this work, a salt bridge was considered to be formed if the minimum distance between the nitrogen atom of side-chain NH_3^+ group of K80 and the side-chain COO^- group of E46 was less than 0.4 nm. The binding affinity of DA/NE molecules to αS tetramer was characterized using contact probability. Here, a contact was defined if the distance between the heavy atoms of DA/NE molecule and αS tetramer lied within 0.54 nm [65,68]. All the representations of the simulated systems were drawn with the VMD program [69].

3. Results and Discussion

3.1. DA/NE Molecules Destabilize αS Protofibril by Disrupting the β-Sheet Structure and Destroying the Intra- and Inter-Peptide E46-K80 Salt Bridges

In order to examine the effect of DA/NE molecules on the structural stability of αS tetramer, we first calculated the root-mean-squared deviation (RMSD) of the Cα atoms of tetramer from the initial structure in the isolated tetramer and tetramer + DA/NE systems as a function of simulation time. It can be seen from Figure 2a,b that all of the MD simulations in the two systems reached equilibrium after 250 ns. Therefore, the analytical parameters below were based on the last 50 ns of data of each MD trajectory. We found that the average RMSD values in the three MD runs of the isolated tetramer system during 250–300 ns were respectively 0.34, 0.32, and 0.32 nm; with the addition of DA/NE, the values changed to 0.35, 0.69, and 0.41 nm. Previous computational studies also reported that $αS_{20/30-110}$ pentamer [70], $αS_{61-95}$ pentamer [71], and $αS_{29-98}$ decamer [72] could maintain the β-sheet structures and display a stable conformation during the MD simulations. The increased RMSD value of αS tetramers with DA/NE molecules compared to those without DA/NE molecules suggested that the binding of DA/NE molecules led to a decreased structural stability of αS tetramer. Figure 2c shows the snapshots of αS tetramer in Run 1 of the tetramer system and Run 2 of the tetramer + DA/NE system, generated at t = 0, 150, and 300 ns. The isolated αS tetramer remained quite stable during the simulation time of 300 ns. In contrast, the binding of DA/NE molecules to αS tetramer enhanced the flexibility of the chains at the edge of the protofibril and led to the departure of the N-terminal fragment of one edge chain. Note that the RMSD of $αS_{44-96}$ cannot represent that of the full length αS, because the N- and C-terminal regions of αS are highly structurally flexible. These results indicate that DA/NE molecules disturb the structural stability of αS tetramer.

**Figure 2.** Structural stability analysis of αS tetramer in the absence and presence of DA/NE molecules. (**a**,**b**) The Cα-RMSD of αS tetramer in the tetramer and tetramer + DA/NE systems as a function of simulation time. (**c**) Snapshots of the tetramer and tetramer + DA/NE systems at 0, 150, and 300 ns. The representations are consistent with those in Figure 1.

To examine the influence of DA/NE molecules on the secondary structure of αS tetramer, we then calculated the probabilities of different secondary structures (coil, β-sheet, β-bridge, bend, and turn) of αS tetramer using the last 50 ns trajectory data. As shown in Figure 3a, with the addition of DA/NE molecules, the average value of β-sheet probability decreased from 45.3% to 35.7%; the average value of coil/bend probabilities increased from 32.9/13.1% to 36.3/15.1%; the probabilities of β-bridge and turn did not change much. These demonstrate that DA/NE molecules can reduce the β-sheet content of αS tetramer and convert part of the β-sheet structure into the random coil or bend conformation. To identify the residues that contribute the most to the β-sheet reduction, we further calculated the β-sheet probability for the individual residue of $αS_{44—96}$ peptides in Figure 3b. It is shown that the β-sheet probabilities of residues V52-V55, T72-V74, Q79-E83, and I88-V95 in the tetramer + DA/NE system were strongly reduced compared to those in the isolated αS tetramer system. The previous NMR study suggested that the fragments T44-V55, E61-G66, V70-A78, T81-E83, and I88-K96 adopt the β-sheet in $αS_{44—96}$ protofibril [39], and the innermost β-sheet of the core including residues 71–82 was reported to be necessary for αS fibril formation [73,74]. These regions are involved in the reduction of β-sheets observed in our simulations, which is supposed to go against αS fibrillation. Overall, DA/NE molecules can serve as a β-sheet breaker to disrupt the β-sheet structures of $αS_{44—96}$ protofibrils.
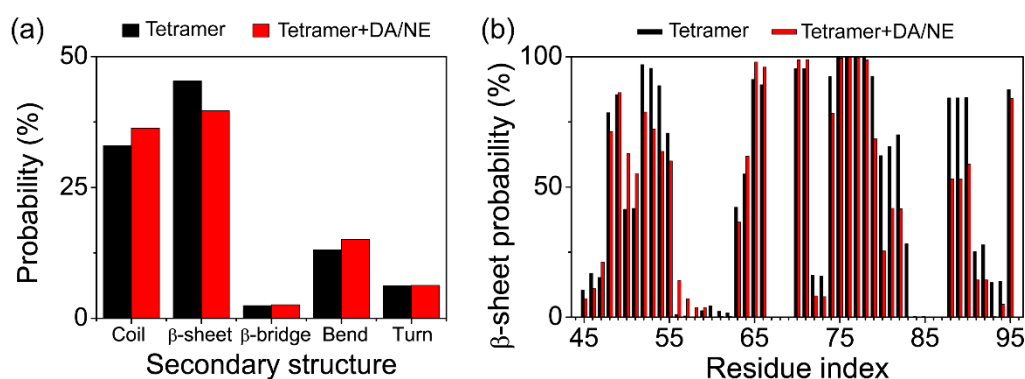
Figure 3. Influence of DA/NE molecules on the secondary structure of αS tetramer. (**a**) Average probabilities of different secondary structures for two simulated systems. (**b**) Residue based β-sheet probability of αS tetramer with and without DA/NE molecules.

As previous experimental and computational studies suggested that E46-K80 salt-bridges are crucial for the stability of αS protofibril [39,75], we examined the influence of DA/NE molecules on the E46-K80 salt-bridges. The probability density function (PDF) of intra- and inter-peptide E46-K80 distance between the side-chain COO^- group of E46 and the N_ζ atom of the side-chain NH_3^+ group of K80 was calculated using the last 50 ns of data of all the MD runs. Figure 4a,b shows the intra-peptide E46-K80 distance distribution. There existed a sharp peak centered at 0.15 nm in the isolated tetramer system, indicating well preserved salt bridges, while the peak value became much smaller in the tetramer + DA/NE system. Figure 4c,d shows the inter-peptide E46-K80 distance distribution. Two peaks centered at 0.15 and 0.45 nm were observed in the isolated tetramer system, while there was a significant reduction of the two peak values in the tetramer + DA/NE system, especially for that at 0.15 nm. These results demonstrate that DA/NE molecules can destroy the intra- and inter-peptide E46-K80 salt bridges, as a result destabilizing αS tetramer protofibril.
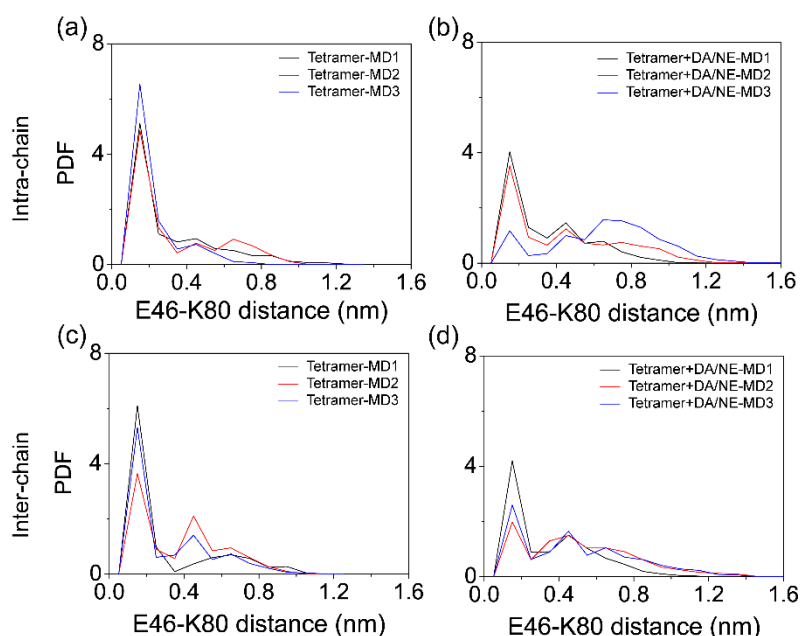
Figure 4. Influence of DA/NE molecules on the intra- and inter-chain E46-K80 salt bridges of αS tetramer. The probability density function (PDF) of the intra-chain (**a**,**b**) and inter-chain (**c**,**d**) E46-K80 distance in the two systems.

3.2. DA/NE Molecules Destroy the Inter-Chain Backbone Hydrogen Bonds, and NE Molecules Form More H-Bonds with αS Tetramer Than DA Molecules

As the backbone H-bonds' formation is closely related to the structural stability and β-sheet formation of αS protofibril, we calculated the distribution of the average inter- and intra-molecular backbone H-bond number for two systems using the last 50 ns of data of each MD trajectory. As shown in Figure 5a, the number of average inter-chain H-bonds was obviously reduced with the addition of DA/NE molecules, and the peak location decreased from 95 to 86. The average intra-chain H-bond number slightly increased with the peak location shifting from eight to 11. Previous MD study on β-amyloid oligomer showed that the disturbance of the inter-peptide H-bonding network and the increment of side-chain H-bonds may result in increased coil content and morphological diversity [76]. The reduction of inter-chain backbone H-bonds of αS protofibril induced by DA/NE molecules is supposed to go against the structural stability of αS protofibril and the subsequent fibrillation. We also calculated the number of H-bonds formed between individual residue and DA/NE molecules. Figure 5b shows that DA and NE molecules mainly form H-bonds with the main chains of residues 55–68 in αS tetramer. DA preferentially forms H-bonds with charged residues K60 and E83 and hydrophobic residue V82; NE forms H-bonds mostly with charged residues K96, E57, and K58. On the whole, NE is more likely to form H-bonds with αS protofibril compared to DA at the same concentration (here, the molar ratio of DA:NE is 1:1).
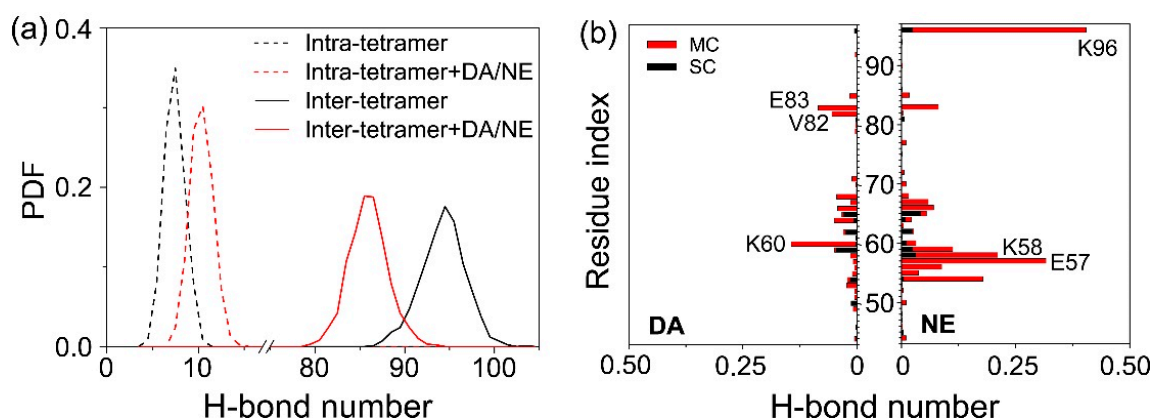

Figure 5. Influence of DA/NE molecules on the H-bond formation in αS tetramer. (**a**) PDF of the average inter-chain and intra-chain H-bond number in the isolated tetramer and tetramer + DA/NE systems. (**b**) Number of main-chain (MC) and side-chain (SC) H-bonds formed between αS tetramer and DA/NE molecules. The results were averaged over the last 50 ns of data of all MD runs.

3.3. The Binding Sites and Interactive Binding Behavior of DA/NE Molecules on αS Tetramer

To identify the binding sites of each neurotransmitter (DA or NE) on αS tetramer, we respectively calculated the residue based binding probability of DA and NE molecules to αS tetramer using the last 50 ns of data of the simulations. As shown in Figure 6, DA molecules had the highest binding probability with polar residues T59 and T64, negatively charged residues E61 and E57, and hydrophobic residue V70; NE molecules had the highest binding probability with polar residue T59, negatively charged E57 and E61, and positively charged K58 and K60. Both DA and NE molecules preferentially bind to the charged residues E57 and E61 and polar residue T59, indicating the important role of electrostatic interaction in the DA/NE–tetramer interaction. The aforementioned calculation of H-bond number shows that the charged residues E57, K58, and K60, as well as the polar residue T59 have a high affinity of forming H-bonds with DA/NE molecules. This reflects that H-bonding interaction also plays a role in the binding of DA/NE molecules to αS tetramer. Small molecules carrying net or partial charges may have a high binding probability with negatively and positively charged residues at the same time [67,77,78]. Besides, we found that DA molecules have a high binding probability

with hydrophobic residue V70. As DA has the polar part (two hydroxyl groups) and nonpolar part (benzene ring), the benzene rings of DA molecules binding to residue V70 were found to be close to the hydrophobic side-chain of V70 through the MD trajectory track, indicating a strong hydrophobic interaction in between. However, NE molecules do not bind to V70 with a high probability, and this difference might be attributed to the lower hydrophilicity of the DA molecule compared to NE, because the DA molecule has one less hydroxyl group. Overall, these results indicate that the electrostatic and H-bonding interactions play dominant roles in the binding of DA/NE molecules to αS tetramer.
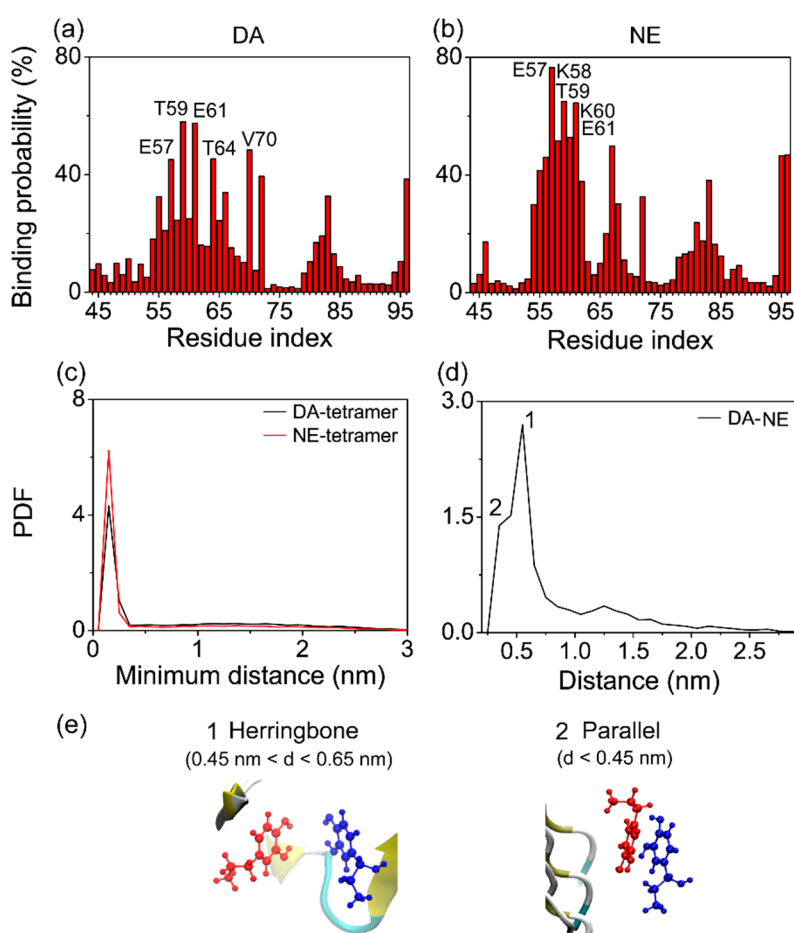
Figure 6. Analysis of αS-DA/NE and DA–NE interactions. (**a**,**b**) Residue based binding probability of DA and NE molecules with αS tetramer. (**c**) PDF of the minimum distance between DA/NE molecules and αS tetramer. (**d**) PDF of the centroid distance between the aromatic ring of DA and the aromatic ring of NE. (**e**) Representative snapshots of the π-stacking patterns of DA with NE molecules. The two patterns correspond to the PDF peaks of the centroid distance between DA and NE aromatic rings, respectively.

According to the residue based binding probability, we identified the favorable binding sites of DA/NE molecules to αS tetramer. DA molecules were found to have a preference to bind at three sites: T54-T72, Q79-A85, and F94-K96. The binding sites of NE molecules on αS tetramer were similar to those of DA, and the binding probability of each site of NE molecules was higher. This implies that NE molecules have a stronger binding capacity to αS tetramer compared to DA at the same concentration. To further confirm this conjecture, we calculated the PDF of the minimum distance between DA/NE molecules and αS tetramer in Figure 6c. The minimum distance distribution displays a sharp peak at a distance of 0.15 nm between NE molecules and αS tetramer, while the peak value is reduced in the DA-tetramer PDF curve. These results indicate that more NE molecules are able to get

closer to αS tetramer than DA molecules when interacting with αS protofibril, leading to a stronger binding strength.

Since DA and NE molecules were reported to be able to interact with each other in the brain [43–45], it is interesting to examine the DA–NE interactions in our simulation systems, and we found that the aromatic-stacking interaction plays an important role in the DA–NE interplay. The PDF of the centroid distance between the DA aromatic ring and the NE aromatic ring is presented in Figure 6d. It can be seen that there is a sharp peak centered at 0.55 nm (labeled 1) and a smaller peak centered at 0.35 nm (labeled 2). The ring orientation calculation between the DA ring and NE ring (not shown) and trajectory tracing indicate that when a DA ring couples with a NE ring, the two rings have a strong preference to be a herringbone if located at a centroid distance of $0.45 < d < 0.65$ nm; they prefer a parallel ring organization if the centroid distance is less than 0.45 nm. The corresponding herringbone and parallel π-stacking patterns between the aromatic rings of DA and NE molecules are shown in the snapshots of Figure 6e. These results imply that DA molecules can bind to αS protofibril through two means: DA is able to bind to the preferential region of αS tetramer directly (Way I), or it can adsorb to the αS-bound NE molecules by π-stacking and bind to αS indirectly (Way II). In addition, DA displayed a high similarity of binding sites to αS protofibril with respect to NE molecules, which means one site would be energetically suitable for the adsorption of both DA and NE molecules. This allows DA and NE molecules to always assist each other in adsorption to αS rather than compete. The situation is the same when NE molecules bind to αS protofibril, and the difference lies in that NE has a stronger binding capacity to αS. Thus, DA and NE molecules bind to αS protofibril interactively.

4. Conclusions

In summary, we investigated the structural influence and binding behavior of DA/NE molecules on the preformed αS protofibrillar tetramer, as well as the underlying disruptive mechanism by performing multiple MD simulations. The increased RMSD value of αS tetramer in the tetramer + DA/NE system shows that DA/NE molecules can disturb the structural stability of αS tetramer. By calculating the secondary structure, we found that DA/NE molecules can disrupt the β-sheet structure of αS tetramer by reducing the β-sheet content of residues V52-V55, T72-V74, Q79-E83, and I88-V95. DA/NE molecules can also reduce the inter-chain H-bond number and destroy the E46-K80 salt bridges. The destabilization of αS protofibril resulting from DA/NE binding is supposed to prevent the peptide–peptide association and inhibit the subsequent fibrillation. Three binding sites were identified for both DA and NE molecules interacting with αS tetramer: T54-T72, Q79-A85, and F94-K96, and NE molecules have a stronger binding capacity to these sites than DA. The binding of DA/NE molecules to αS tetramer is dominantly driven by the electrostatic and H-bonding interactions. Through aromatic π-stacking, DA and NE molecules may bind to αS protofibril interactively. Overall, our work provides the molecular details of the disruptive effects of DA/NE molecules on αS protofibrillar oligomer, which is helpful for developing new treatments (drug design or exercise therapy) against PD.

Author Contributions: Conceptualization, Z.Q.; data curation, Y.Z. and Z.L.; investigation, Z.L. and Z.Z.; methodology, Z.L.; validation, Z.Z.; writing, original draft, Y.Z.; writing, review and editing, Z.Q.

References

1. Chiti, F.; Dobson, C.M. Protein misfolding, functional amyloid, and human disease. *Annu. Rev. Biochem.* **2006**, *75*, 333–366. [CrossRef] [PubMed]
2. Chiti, F.; Dobson, C.M. Protein misfolding, amyloid formation, and human disease: A summary of progress over the last decade. *Annu. Rev. Biochem.* **2017**, *86*, 27–68. [CrossRef] [PubMed]

3. Eisenberg, D.S.; Sawaya, M.R. Structural studies of amyloid proteins at the molecular level. *Annu. Rev. Biochem.* **2017**, *86*, 69–95. [CrossRef] [PubMed]

4. Spillantini, M.G.; Schmidt, M.L.; Lee, V.M.; Trojanowski, J.Q.; Jakes, R.; Goedert, M. Alpha-synuclein in Lewy bodies. *Nature* **1997**, *388*, 839–840. [CrossRef] [PubMed]

5. Baba, M.; Nakajo, S.; Tu, P.H.; Tomita, T.; Nakaya, K.; Lee, V.M.; Trojanowski, J.Q.; Iwatsubo, T. Aggregation of alpha-synuclein in Lewy bodies of sporadic Parkinson's disease and dementia with Lewy bodies. *Am. J. Pathol.* **1998**, *152*, 879–884. [PubMed]

6. Serpell, L.C.; Berriman, J.; Jakes, R.; Goedert, M.; Crowther, R.A. Fiber diffraction of synthetic alpha-synuclein filaments shows amyloid-like cross-beta conformation. *Proc. Natl. Acad. Sci. USA* **2000**, *97*, 4897–4902. [CrossRef]

7. Nelson, R.; Sawaya, M.R.; Balbirnie, M.; Madsen, A.O.; Riekel, C.; Grothe, R.; Eisenberg, D. Structure of the cross-beta spine of amyloid-like fibrils. *Nature* **2005**, *435*, 773–778. [CrossRef]

8. Stefani, M.; Dobson, C.M. Protein aggregation and aggregate toxicity: New insights into protein folding, misfolding diseases and biological evolution. *J. Mol. Med.* **2003**, *81*, 678–699. [CrossRef]

9. Gillam, J.E.; MacPhee, C.E. Modelling amyloid fibril formation kinetics: Mechanisms of nucleation and growth. *J. Phys. Condens. Matter* **2013**, *25*, 373101. [CrossRef]

10. Lashuel, H.A.; Petre, B.M.; Wall, J.; Simon, M.; Nowak, R.J.; Walz, T.; Lansbury, P.T., Jr. Alpha-synuclein, especially the Parkinson's disease-associated mutants, forms pore-like annular and tubular protofibrils. *J. Mol. Biol.* **2002**, *322*, 1089–1102. [CrossRef]

11. Ingelsson, M. Alpha-synuclein oligomers-neurotoxic molecules in Parkinson's disease and other Lewy body disorders. *Front. Neurosci.* **2016**, *10*, 408. [CrossRef] [PubMed]

12. El-Agnaf, O.M.; Paleologou, K.E.; Greer, B.; Abogrein, A.M.; King, J.E.; Salem, S.A.; Fullwood, N.J.; Benson, F.E.; Hewitt, R.; Ford, K.J.; et al. A strategy for designing inhibitors of alpha-synuclein aggregation and toxicity as a novel treatment for Parkinson's disease and related disorders. *FASEB J.* **2004**, *18*, 1315–1317. [CrossRef] [PubMed]

13. Kim, Y.S.; Lim, D.; Kim, J.Y.; Kang, S.J.; Kim, Y.H.; Im, H. Beta-sheet-breaking peptides inhibit the fibrillation of human alpha-synuclein. *Biochem. Biophys. Res. Commun.* **2009**, *387*, 682–687. [CrossRef] [PubMed]

14. Bieschke, J.; Russ, J.; Friedrich, R.P.; Ehrnhoefer, D.E.; Wobst, H.; Neugebauer, K.; Wanker, E.E. EGCG remodels mature alpha-synuclein and amyloid-beta fibrils and reduces cellular toxicity. *Proc. Natl. Acad. Sci. USA* **2010**, *107*, 7710–7715. [CrossRef]

15. Ahsan, N.; Mishra, S.; Jain, M.K.; Surolia, A.; Gupta, S. Curcumin pyrazole and its derivative (N-(3-Nitrophenylpyrazole) curcumin inhibit aggregation, disrupt fibrils and modulate toxicity of wild type and mutant alpha-synuclein. *Sci. Rep.* **2015**, *5*, 9862. [CrossRef]

16. Iljina, M.; Hong, L.; Horrocks, M.H.; Ludtmann, M.H.; Choi, M.L.; Hughes, C.D.; Ruggeri, F.S.; Guilliams, T.; Buell, A.K.; Lee, J.E.; et al. Nanobodies raised against monomeric a-synuclein inhibit fibril formation and destabilize toxic oligomeric species. *BMC Biol.* **2017**, *15*, 57. [CrossRef]

17. Li, X.; Koudstaal, W.; Fletcher, L.; Costa, M.; van Winsen, M.; Siregar, B.; Inganas, H.; Kim, J.; Keogh, E.; Macedo, J.; et al. Naturally occurring antibodies isolated from PD patients inhibit synuclein seeding in vitro and recognize Lewy pathology. *Acta Neuropathol.* **2019**, *137*, 825–836. [CrossRef]

18. Kim, D.; Yoo, J.M.; Hwang, H.; Lee, J.; Lee, S.H.; Yun, S.P.; Park, M.J.; Lee, M.; Choi, S.; Kwon, S.H.; et al. Graphene quantum dots prevent alpha-synucleinopathy in Parkinson's disease. *Nat. Nanotechnol.* **2018**, *13*, 812–818. [CrossRef]

19. Sun, Y.; Kakinen, A.; Zhang, C.; Yang, Y.; Faridi, A.; Davis, T.P.; Cao, W.; Ke, P.C.; Ding, F. Amphiphilic surface chemistry of fullerenols is necessary for inhibiting the amyloid aggregation of alpha-synuclein NACore. *Nanoscale* **2019**, *11*, 11933–11945. [CrossRef]

20. Venda, L.L.; Cragg, S.J.; Buchman, V.L.; Wade-Martins, R. Alpha-synuclein and dopamine at the crossroads of Parkinson's disease. *Trends Neurosci.* **2010**, *33*, 559–568. [CrossRef]

21. Bisaglia, M.; Filograna, R.; Beltramini, M.; Bubacco, L. Are dopamine derivatives implicated in the pathogenesis of Parkinson's disease? *Ageing Res. Rev.* **2014**, *13*, 107–114. [CrossRef] [PubMed]

22. Delaville, C.; Deurwaerdere, P.D.; Benazzouz, A. Noradrenaline and Parkinson's disease. *Front. Syst. Neurosci.* **2011**, *5*, 31. [CrossRef] [PubMed]

23. Espay, A.J.; LeWitt, P.A.; Kaufmann, H. Norepinephrine deficiency in Parkinson's disease: The case for noradrenergic enhancement. *Mov. Disord.* **2014**, *29*, 1710–1719. [CrossRef] [PubMed]

24. Conway, K.A.; Rochet, J.C.; Bieganski, R.M.; Lansbury, P.T., Jr. Kinetic stabilization of the alpha-synuclein protofibril by a dopamine-alpha-synuclein adduct. *Science* **2001**, *294*, 1346–1349. [CrossRef]

25. Li, J.; Zhu, M.; Manning-Bog, A.B.; Di Monte, D.A.; Fink, A.L. Dopamine and L-dopa disaggregate amyloid fibrils: Implications for Parkinson's and Alzheimer's disease. *FASEB J.* **2004**, *18*, 962–964. [CrossRef]

26. Cappai, R.; Leck, S.L.; Tew, D.J.; Williamson, N.A.; Smith, D.P.; Galatis, D.; Sharples, R.A.; Curtain, C.C.; Ali, F.E.; Cherny, R.A.; et al. Dopamine promotes alpha-synuclein aggregation into SDS-resistant soluble oligomers via a distinct folding pathway. *FASEB J.* **2005**, *19*, 1377–1379. [CrossRef]

27. Herrera, F.E.; Chesi, A.; Paleologou, K.E.; Schmid, A.; Munoz, A.; Vendruscolo, M.; Gustincich, S.; Lashuel, H.A.; Carloni, P. Inhibition of alpha-synuclein fibrillization by dopamine is mediated by interactions with five C-terminal residues and with E83 in the NAC region. *PLoS ONE* **2008**, *3*, e3394. [CrossRef]

28. Latawiec, D.; Herrera, F.; Bek, A.; Losasso, V.; Candotti, M.; Benetti, F.; Carlino, E.; Kranjc, A.; Lazzarino, M.; Gustincich, S.; et al. Modulation of alpha-synuclein aggregation by dopamine analogs. *PLoS ONE* **2010**, *5*, e9234. [CrossRef]

29. Ono, K.; Takasaki, J.; Takahashi, R.; Ikeda, T.; Yamada, M. Effects of antiparkinsonian agents on beta-amyloid and alpha-synuclein oligomer formation in vitro. *J. Neurosci. Res.* **2013**, *91*, 1371–1381. [CrossRef]

30. Tavassoly, O.; Nokhrin, S.; Dmitriev, O.Y.; Lee, J.S. Cu(II) and dopamine bind to alpha-synuclein and cause large conformational changes. *FEBS J.* **2014**, *281*, 2738–2753. [CrossRef]

31. Jain, M.K.; Bhat, R. Modulation of human alpha-synuclein aggregation by a combined effect of calcium and dopamine. *Neurobiol. Dis.* **2014**, *63*, 115–128. [CrossRef] [PubMed]

32. Fischer, A.F.; Matera, K.M. Stabilization of alpha-synuclein oligomers in vitro by the neurotransmitters, dopamine and norepinephrine: The effect of oxidized catecholamines. *Neurochem. Res.* **2015**, *40*, 1341–1349. [CrossRef] [PubMed]

33. Jha, N.N.; Kumar, R.; Panigrahi, R.; Navalkar, A.; Ghosh, D.; Sahay, S.; Mondal, M.; Kumar, A.; Maji, S.K. Comparison of alpha-synuclein fibril inhibition by four different amyloid inhibitors. *ACS Chem. Neurosci.* **2017**, *8*, 2722–2733. [CrossRef]

34. Fink, A.L. The aggregation and fibrillation of alpha-synuclein. *Acc. Chem. Res.* **2006**, *39*, 628–634. [CrossRef]

35. Illes-Toth, E.; Dalton, C.F.; Smith, D.P. Binding of dopamine to alpha-synuclein is mediated by specific conformational states. *J. Am. Soc. Mass Spectrom.* **2013**, *24*, 1346–1354. [CrossRef]

36. Pham, C.L.; Cappai, R. The interplay between lipids and dopamine on alpha-synuclein oligomerization and membrane binding. *Biosci. Rep.* **2013**, *33*, e00074. [CrossRef]

37. Singh, P.; Bhat, R. Binding of noradrenaline to native and intermediate states during the fibrillation of alpha-synuclein leads to the formation of stable and structured cytotoxic species. *ACS Chem. Neurosci.* **2019**, *10*, 2741–2755. [CrossRef]

38. Khalife, M.; Morshedi, D.; Aliakbari, F.; Tayaranian Marvian, A.; Mohammad Beigi, H.; Azimzadeh Jamalkandi, S.; Pan-Montojo, F. Alpha-synuclein fibrils interact with dopamine reducing its cytotoxicity on PC12 cells. *Protein J.* **2015**, *34*, 291–303. [CrossRef]

39. Tuttle, M.D.; Comellas, G.; Nieuwkoop, A.J.; Covell, D.J.; Berthold, D.A.; Kloepper, K.D.; Courtney, J.M.; Kim, J.K.; Barclay, A.M.; Kendall, A.; et al. Solid-state NMR structure of a pathogenic fibril of full-length human alpha-synuclein. *Nat. Struct. Mol. Biol.* **2016**, *23*, 409–415. [CrossRef]

40. Yamaguchi, Y.; Masuda, M.; Sasakawa, H.; Nonaka, T.; Hanashima, S.; Hisanaga, S.; Kato, K.; Hasegawa, M. Characterization of inhibitor-bound alpha-synuclein dimer: Role of alpha-synuclein N-terminal region in dimerization and inhibitor binding. *J. Mol. Biol.* **2010**, *395*, 445–456. [CrossRef]

41. Dibenedetto, D.; Rossetti, G.; Caliandro, R.; Carloni, P. A molecular dynamics simulation-based interpretation of nuclear magnetic resonance multidimensional heteronuclear spectra of alpha-synuclein.dopamine adducts. *Biochemistry* **2013**, *52*, 6672–6683. [CrossRef] [PubMed]

42. Corvaglia, S.; Sanavio, B.; Hong Enriquez, R.P.; Sorce, B.; Bosco, A.; Scaini, D.; Sabella, S.; Pompa, P.P.; Scoles, G.; Casalis, L. Atomic force microscopy based nanoassay: A new method to study alpha-Synuclein-dopamine bioaffinity interactions. *Sci. Rep.* **2014**, *4*, 5366. [CrossRef] [PubMed]

43. Ponzio, F.; Hallman, H.; Jonsson, G. Noradrenaline and dopamine interaction in rat brain during development. *Med. Biol.* **1981**, *59*, 161–169. [PubMed]

44. Colpaert, F.C. Pharmacological characteristics of tremor, rigidity and hypokinesia induced by reserpine in rat. *Neuropharmacology* **1987**, *26*, 1431–1440. [CrossRef]

45. Taylor, T.N.; Caudle, W.M.; Shepherd, K.R.; Noorian, A.; Jackson, C.R.; Iuvone, P.M.; Weinshenker, D.; Greene, J.G.; Miller, G.W. Nonmotor symptoms of Parkinson's disease revealed in an animal model with reduced monoamine storage capacity. *J. Neurosci.* **2009**, *29*, 8103–8113. [CrossRef] [PubMed]

46. Schüttelkopf, A.W.; Van Aalten, D.M.F. PRODRG: A tool for high-throughput crystallography of protein-ligand complexes. *Acta Crystallogr. D Biol. Crystallogr.* **2004**, *60*, 1355–1363. [CrossRef]

47. Shao, Y.; Molnar, L.; Jung, Y.; Kussmann, J.; Ochsenfeld, C.; Brown, S.; Gilbert, A.; Slipchenko, L.; Levchenko, S.; O'Neill, D.; et al. Advances in methods and algorithms in a modern quantum chemistry program package. *Phys. Chem. Chem. Phys.* **2006**, *8*, 3172–3191. [CrossRef]

48. Schmidt, M.W.; Baldridge, K.K.; Boatz, J.A.; Elbert, S.T.; Gordon, M.S.; Jensen, J.H.; Koseki, S.; Matsunaga, N.; Nguyen, K.A.; Su, S. General atomic and molecular electronic structure system. *J. Comput. Chem.* **1993**, *14*, 1347–1363. [CrossRef]

49. François-Yves, D.; Adrien, P.; Thomas, Z.; Corentin, S.; Rodolphe, L.; Nicolas, G.; Dimitri, L.; Wilfried, R.; Piotr, C. The R.E.D. tools: Advances in RESP and ESP charge derivation and force field library building. *Phys. Chem. Chem. Phys.* **2010**, *12*, 7821–7839.

50. Corona-Avendano, S.; Alarcon-Angeles, G.; Rosquete-Pina, G.A.; Rojas-Hernandez, A.; Gutierrez, A.; Ramirez-Silva, M.T.; Romero-Romo, M.; Palomar-Pardave, M. New insights on the nature of the chemical species involved during the process of dopamine deprotonation in aqueous solution: Theoretical and experimental study. *J. Phys. Chem. B* **2007**, *111*, 1640–1647. [CrossRef]

51. Farley, I.J.; Hornykiewicz, O. Noradrenaline distribution insubcortical areas of the human brain. *Brain Res.* **1977**, *126*, 53–62. [CrossRef]

52. Hardy, J.A.; Wester, P.; Backstrom, I.; Gottfries, J.; Oreland, L.; Stenstrom, A.; Winblad, B. The regional distribution of dopamine and serotonin uptake and transmitter concentrations in the human brain. *Neurochem. Int.* **1987**, *10*, 445–450. [CrossRef]

53. Van, D.S.D.; Lindahl, E.; Hess, B.; Groenhof, G.; Mark, A.E.; Berendsen, H.J. GROMACS: Fast, flexible, and free. *J. Comput. Chem.* **2005**, *26*, 1701–1718.

54. Lindorff-Larsen, K.; Piana, S.; Palmo, K.; Maragakis, P.; Klepeis, J.L.; Dror, R.O.; Shaw, D.E. Improved side-chain torsion potentials for the Amber ff99SB protein force field. *Proteins* **2010**, *78*, 1950–1958. [CrossRef] [PubMed]

55. Jorgensen, W.L.; Chandrasekhar, J.; Madura, J.D.; Impey, R.W.; Klein, M.L. Comparison of simple potential functions for simulating liquid water. *J. Chem. Phys.* **1983**, *79*, 926–935. [CrossRef]

56. Hess, B.; Bekker, H.; Berendsen, H.J.; Fraaije, J.G. LINCS: A linear constraint solver for molecular simulations. *J. Comput. Chem.* **1997**, *18*, 1463–1472. [CrossRef]

57. Miyamoto, S.; Kollman, P.A. Settle: An analytical version of the SHAKE and RATTLE algorithm for rigid water models. *J. Comput. Chem.* **1992**, *13*, 952–962. [CrossRef]

58. Parrinello, M.; Rahman, A. Polymorphic transitions in single crystals: A new molecular dynamics method. *J. Appl. Phys.* **1981**, *52*, 7182–7190. [CrossRef]

59. Darden, T.; York, D.; Pedersen, L. Particle mesh Ewald: An N·log(N) method for Ewald sums in large systems. *J. Chem. Phys.* **1998**, *98*, 10089–10092. [CrossRef]

60. Kabsch, W.; Sander, C. Dictionary of protein secondary structure: Pattern recognition of hydrogen-bonded and geometrical features. *Biopolymers* **1983**, *22*, 2577–2637. [CrossRef] [PubMed]

61. Barlow, D.J.; Thornton, J.M. Ion-pairs in proteins. *J. Mol. Biol.* **1983**, *168*, 867–885. [CrossRef]

62. Kumar, S.; Nussinov, R. Salt bridge stability in monomeric proteins. *J. Mol. Biol.* **1999**, *293*, 1241–1255. [CrossRef]

63. Kumar, S.; Nussinov, R. Close-range electrostatic interactions in proteins. *ChemBioChem* **2002**, *3*, 604–617. [CrossRef]

64. Luo, Y.; Ma, B.; Nussinov, R.; Wei, G. Structural insight into tau protein's paradox of intrinsically disordered behavior, self-acetylation activity, and aggregation. *J. Phys. Chem. Lett.* **2014**, *5*, 3026–3031. [CrossRef] [PubMed]

65. Qian, Z.; Zou, Y.; Zhang, Q.; Chen, P.; Ma, B.; Wei, G.; Nussinov, R. Atomistic-level study of the interactions between hIAPP protofibrils and membranes: Influence of pH and lipid composition. *Biochim. Biophys. Acta Biomembr.* **2018**, *1860*, 1818–1825. [CrossRef] [PubMed]

66. Lei, J.; Qi, R.; Tang, Y.; Wang, W.; Wei, G.; Nussinov, R.; Ma, B. Conformational stability and dynamics of the cancer-associated isoform Delta133p53beta are modulated by p53 peptides and p53-specific DNA. *FASEB J.* **2019**, *33*, 4225–4235. [CrossRef] [PubMed]

67. Jin, Y.; Sun, Y.; Chen, Y.; Lei, J.; Wei, G. Molecular dynamics simulations reveal the mechanism of graphene oxide nanosheet inhibition of Abeta1-42 peptide aggregation. *Phys. Chem. Chem. Phys.* **2019**, *21*, 10981–10991. [CrossRef]

68. Liu, Z.; Zou, Y.; Zhang, Q.; Chen, P.; Liu, Y.; Qian, Z. Distinct binding dynamics, sites and interactions of fullerene and fullerenols with amyloid-beta peptides revealed by molecular dynamics simulations. *Int. J. Mol. Sci.* **2019**, *20*, 2048. [CrossRef]

69. Humphrey, W.; Dalke, A.; Schulten, K. VMD: Visual molecular dynamics. *J. Mol. Graph. Model.* **1996**, *14*, 33–38. [CrossRef]

70. Xu, L.; Nussinov, R.; Ma, B. Coupling of the non-amyloid-component (NAC) domain and the KTK(E/Q)GV repeats stabilize the alpha-synuclein fibrils. *Eur. J. Med. Chem.* **2016**, *121*, 841–850. [CrossRef]

71. Xu, L.; Bhattacharya, S.; Thompson, D. The fold preference and thermodynamic stability of alpha-synuclein fibrils is encoded in the non-amyloid-beta component region. *Phys. Chem. Chem. Phys.* **2018**, *20*, 4502–4512. [CrossRef] [PubMed]

72. Romo, T.D.; Lewis, A.K.; Braun, A.R.; Grossfield, A.; Sachs, J.N. Minimal Nucleation State of alpha-Synuclein Is Stabilized by Dynamic Threonine-Water Networks. *ACS Chem. Neurosci.* **2017**, *8*, 1859–1864. [CrossRef] [PubMed]

73. Giasson, B.I.; Murray, I.V.; Trojanowski, J.Q.; Lee, V.M. A hydrophobic stretch of 12 amino acid residues in the middle of alpha-synuclein is essential for filament assembly. *J. Biol. Chem.* **2001**, *276*, 2380–2386. [CrossRef] [PubMed]

74. Bedard, L.; Lefevre, T.; Morin-Michaud, E.; Auger, M. Besides fibrillization: Putative role of the peptide fragment 71-82 on the structural and assembly behavior of alpha-synuclein. *Biochemistry* **2014**, *53*, 6463–6472. [CrossRef] [PubMed]

75. Sanjeev, A.; Mattaparthi, V.S.K. Investigation on the molecular interactions stabilizing the structure of alpha-synuclein fibril: An in silico study. *Cent. Nerv. Syst. Agents Med. Chem.* **2017**, *17*, 209–218. [CrossRef] [PubMed]

76. Qian, Z.; Zhang, Q.; Liu, Y.; Chen, P. Assemblies of amyloid-beta30-36 hexamer and its G33V/L34T mutants by replica-exchange molecular dynamics simulation. *PLoS ONE* **2017**, *12*, e0188794. [CrossRef]

77. Liu, X.; Zhou, S.; Shi, D.; Bai, Q.; Liu, H.; Yao, X. Influence of EGCG on alpha-synuclein (alphaS) aggregation and identification of their possible binding mode: A computational study using molecular dynamics simulation. *Chem. Biol. Drug Des.* **2018**, *91*, 162–171. [CrossRef]

78. Mo, Y.; Brahmachari, S.; Lei, J.; Gilead, S.; Tang, Y.; Gazit, E.; Wei, G. The inhibitory effect of hydroxylated carbon nanotubes on the aggregation of human islet amyloid polypeptide revealed by a combined computational and experimental study. *ACS Chem. Neurosci.* **2018**, *9*, 2741–2752. [CrossRef]